Eur. Phys. J. B (2018) 91: 154
https://doi.org/10.1140/epjb/e2018-90094-8

THE EUROPEAN PHYSICAL JOURNAL B

Regular Article

Geometric symmetry modulated spin polarization of electron transport in graphene-like zigzag FeB_2 nanoribbons

Jian-Hua Li[1,2], Yan-Dong Guo[1,2,a], Xiao-Hong Yan[1,2,3,b], Hong-Li Zeng[1], Xiao-Chen Song[1], and Xin-Yi Mou[1]

[1] College of Electronic and Optical Engineering, Nanjing University of Posts and Telecommunications, Nanjing 210046, P.R. China
[2] Key Laboratory of Radio Frequency and Micro-Nano Electronics of Jiangsu Province, Nanjing 210023, P.R. China
[3] School of Material Science and Engineering, Jiangsu University, Zhenjiang 212013, P.R. China

Received 26 February 2018 / Received in final form 14 May 2018
Published online 4 July 2018

Abstract. Due to electron deficiency, the graphene-like honeycomb structure of boron is unstable. By introducing Fe atoms, it is reported that FeB_2 monolayer has excellent dynamic and thermal stabilities at room temperature. Based on first-principles calculations, the spin-dependent transport of zigzag FeB_2 nanoribbons ($ZFeB_2NRs$) under ferromagnetic state (FM) is investigated. It is found that, around the Fermi level, FeB-terminated (or FeFe-terminated) $ZFeB_2NRs$ exhibit completely spin-polarized (or spin-unpolarized) transmission, and BB-terminated configurations exhibit completely unpolarized or partially polarized transmission. Further analysis shows that, the hinge dihedral angle has a switching effect on the transport channels, and the spin polarization of the transmission is determined by the symmetry of the distribution of hinge dihedral angles along the transverse direction of the ribbon, where symmetric/asymmetric distribution induces spin-unpolarized/polarized transmission. Moreover, such a symmetry effect is found to be robust to the width of the ribbon, showing great application potential. Our findings may throw light on the development of B-based spintronic devices.

1 Introduction

Spintronics have attracted significant attention, and it becomes a promising field for future nanoelectronics [1–3]. One of the key points in this area is the manipulation of a spin current. Due to the need for large-scale integration, it is quite beneficial to use two-dimensional (2D) nanomaterials. Up to now, great achievements have been made in 2D structures, e.g., graphene [4–8]. Meanwhile, the search for new monolayer 2D structures has never stopped. Recently, as an analogue of graphene, borophene is synthesized atomically thin in experiment [9,10]. However, due to the electron deficiency, hexagonal boron structure is unstable. By introducing Fe atoms, Zhang et al. [11] reported that monolayer FeB_2 exhibits excellent dynamic and thermal stabilities, which still preserves the honeycomb geometry. As well known, in 2D systems, the edge generally has great influence on the electronic structure [12–15]. In particular, zigzag edge usually makes the system acquire magnetism and also plays an important role in the spin-related transport [16,17]. Unlike graphene ribbon, there are two kinds of edges in zigzag FeB_2 nanoribbons ($ZFeB_2NRs$), i.e., Fe- or B-terminated ones. Due to the involving of Fe atoms, 2D honeycomb structure of FeB_2 is found to exhibit intrinsic magnetism [11]. So, because of the existence of the interplay between edges' and Fe atoms' magnetism, interesting spin-dependent transport in zigzag FeB_2 nanoribbons ($ZFeB_2NRs$) could be expected.

In the present work, we focus on the spin-dependent electronic transport of $ZFeB_2NRs$ under ferromagnetic state (FM). It is found that FeB-terminated $ZFeB_2NRs$ exhibit completely spin-polarized transmission, while FeFe- and BB-terminated ones exhibit completely or partially spin-unpolarized transmission, depending on the geometry of the ribbon. Further analysis shows that, the spin polarization of the transmission is mainly determined by the symmetry of the hinge dihedral angles' distribution along the transverse direction of the ribbon. Moreover, the symmetry-effect is found to be robust to the width of the ribbon, showing great application potential. We believe our results are quite beneficial for the development of boron-based spintronic devices [18].

2 Computational details

The calculations in our investigation are carried out using the first-principles method based on the combination of

[a] e-mail: yandongguo@njupt.edu.cn
[b] e-mail: yanxh@njupt.edu.cn

the density-functional theory (DFT) and non-equilibrium Green's function (NEGF) [19–23], which are implemented in the Atomistix Toolkit (ATK) package [24]. The electron exchange correlation functional is treated by generalized gradient approximation (GGA) in the form proposed by Perdew, Burke, and Ernzerhof (PBE) [25,26]. The wave functions of all atoms are expanded using double-zeta plus polarization (DZP) basis set. The $1\times1\times31$ k-points Monkhorst-Pack grid is used to calculate the density of states (DOS). The structural models for $ZFeB_2NRs$ have a sufficient vacuum space (more than 10 Å) in the x or y direction to eliminate the interactions between adjacent layers. The structures are fully relaxed until the force on each atom is less then 0.02 eV/Å. The $1 \times 1 \times 100$ k-points mesh is employed in the transport calculation. In the NEGF scheme, the spin-dependent transmission probability through the two-probe system is calculated by

$$T_{\uparrow/\downarrow}(E) = Tr[\Gamma_L(E)G^R_{\uparrow/\downarrow}(E)\Gamma_R(E)G^A_{\uparrow/\downarrow}(E)], \quad (1)$$

where $G^{A/R}_{\uparrow/\downarrow}(E)$ is the spin-dependent advanced or retarded Green's function for the scattering region (E represents energy), and $\Gamma_{L/R}$ is the coupling matrix between this region and the left/right electrode. For instance, $T_\uparrow(E)$ stands for the probability that an up-spin electron with energy E transmits from one electrode to another (it will become a ratio for many electrons).

3 Results and discussions

The geometry of infinite FeB_2 monolayer is similar to graphene with the hexagonal structure. Fe atoms are located above the center of hexagonal boron rings (a height of 0.6 Å in the out-of-plane direction). By cutting, there will be three possible categories of zigzag nanoribbons, i.e., the FeFe-(both edges are Fe-terminated), BB-(both edges are B-terminated) and FeB-terminated (one edge is Fe-terminated and the other is B-terminated) ones. In each category, according to the geometry, the nanoribbons could be divided into two groups, i.e., symmetric (there exists a mirror plane σ, as shown in Fig. 1a) and asymmetric ones (like Fig. 1b), denoted by subscript "sy" and "as" respectively. The ribbon width is represented by N, which is defined as the (largest) number of atoms in each line in the transverse direction. As an example, FeB_{as}@7-$ZFeB_2NR$ stands for the asymmetric FeB-terminated zigzag FeB_2 nanoribbon with the width of $N = 7$, as shown in Figure 1b.

To investigate the electronic transport of the ribbon, two-probe system is constructed, as shown in Figure 1c. It consists of scattering region and semi-infinte left and right leads, where the black solid arrow z refers to the transport direction. As the zero-bias condition is sufficiently enough to represent the small finite bias condition [27,28], in this work, we focus on the zero-bias condition and pay attention to the spin-dependent transport. For all the three terminated-edge categories, we construct both symmetric and asymmetric configurations,

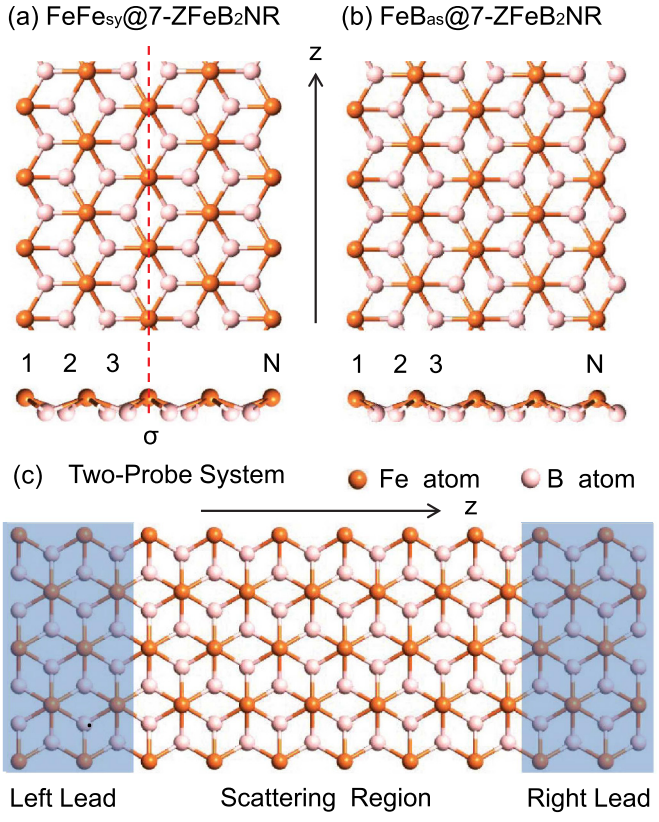

Fig. 1. The zigzag monolayer FeB_2 nanoribbons. (a) The structure of symmetric $FeFe_{sy}$@7-$ZFeB_2NR$. (b) The structure of asymmetric FeB_{as}@7-$ZFeB_2NR$. (c) The two-probe system of $ZFeB_2NR$.

i.e., BB_{as}@5-$ZFeB_2NR$, BB_{as}@7-$ZFeB_2NR$, BB_{sy}@8-$ZFeB_2NR$, FeB_{as}@6-$ZFeB_2N$-R, FeB_{as}@7-$ZFeB_2NR$, FeB_{as}@9-$ZFeB_2NR$, $FeFe_{as}$@5-ZFe-B_2NR and $FeFe_{sy}$@7-$ZFeB_2NR$, shown in the insets of Figures 2a–2d and 2i–2l, respectively.

As the FM state could be easily stabilized in experiment, we limit our work in this state [29,30]. For each configuration, the spin-resolved transmission spectra (it is based on the Landauer formula [31]) are calculated and plotted in Figure 2. In a two-probe system, electronic transport is mainly determined by the transmission around E_F, which is set to be the zero energy in this work.

One finds that, for all the systems, the transmission are not spin-independent, i.e., spin up and down ones do not coincide. They exhibit the morphology of steps, and the transmission coefficients are integer values. For the configurations in Figures 2a, 2b, 2d, 2i and 2j, the transmission of spin down is larger than that of spin up around E_F. As a result, the electron transmission of them is spin polarized. Especially, for the configurations in Figures 2d, 2i and 2j, the transmission of the spin up goes down to zero around E_F. For these configurations, the transmission is completely spin polarized. However, for the configurations in Figures 2c, 2k and 2l, the transmission coefficients for spin up and down are the same around E_F, which means the transmission is completely unpolarized. For clarity, we here define the spin polarization

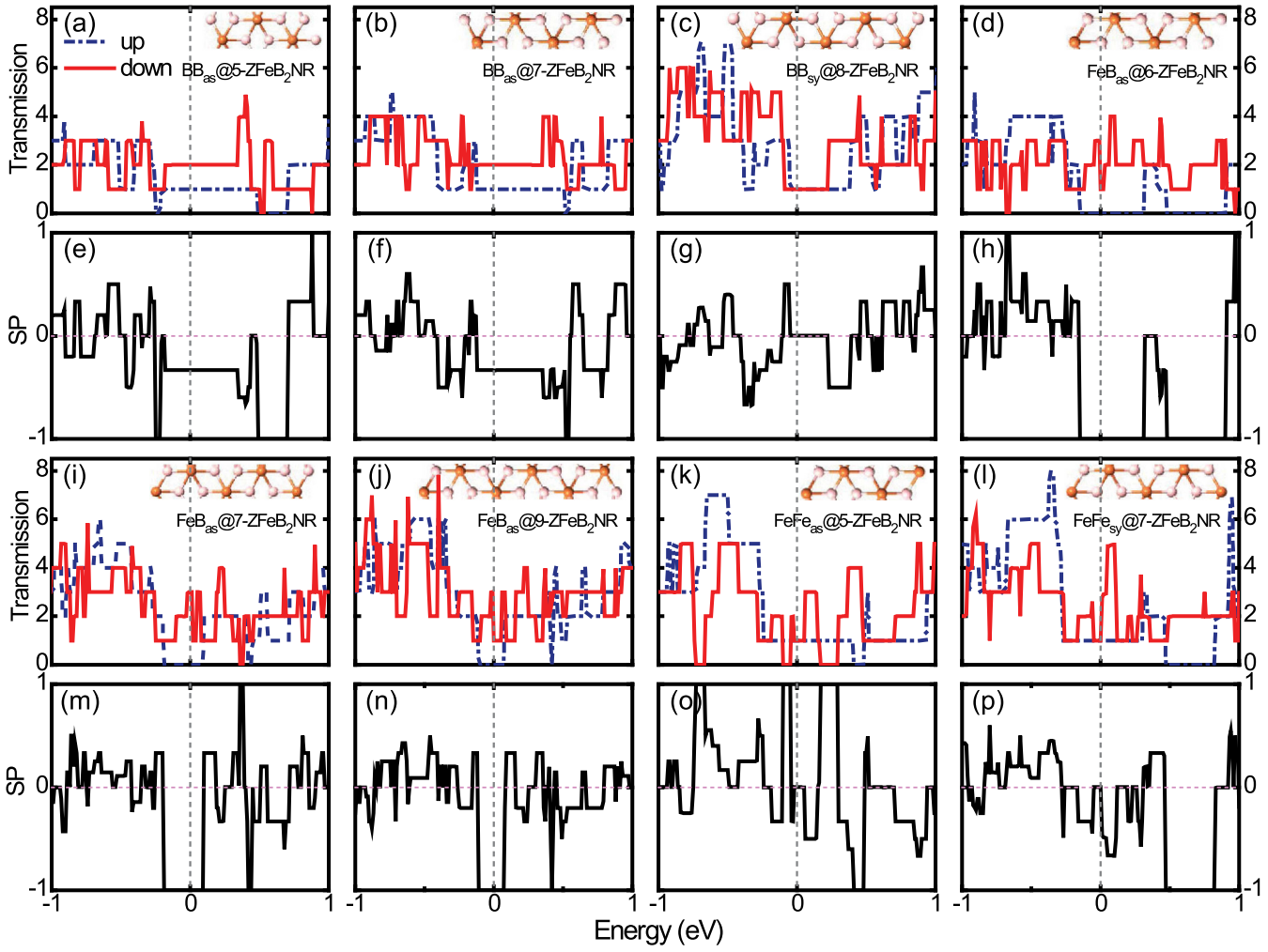

Fig. 2. (a–p) Transmission spectra for BB_{as}@5-$ZFeB_2$NR, BB_{as}@7-$ZFeB_2$NR, BB_{sy}@8-$ZFeB_2$NR, FeB_{as}@6-$ZFeB_2$NR, FeB_{as}@7-$ZFeB_2$NR, FeB_{as}@9-$ZFeB_2$NR, $FeFe_{as}$@5-$ZFeB_2$NR and $FeFe_{sy}$@7-$ZFeB_2$NR respectively. The corresponding spin polarization is shown below the transmission spectra for each case. The blue dash dot line denotes spin up transmission, and red solid line denotes spin down transmission.

as $SP = [(T_{up} - T_{down})/(T_{up} + T_{down})] \times 100\%$ [32]. Thus, $SP = \pm 100\%$ denotes completely spin polarized transmission, and $SP = 0$ denotes completely spin unpolarized state. Other cases between them are partially polarized. For each configuration, we calculate its SP and plot it beside the transmission spectrum, as shown in Figure 2. For the configurations in Figures 2d, 2i and 2j, the SPs around E_F are all –100%, which exhibits completely spin polarized transmission, as shown in Figures 2h, 2m and 2n. In particular, for the configuration in Figure 2d, it shows –100% of SP within the energy rang of [–0.15, 0.31] eV, as shown in Figure 2h. As well known, large SP has good application potential in nanoelectronic devices [33]. However, for the configurations in Figures 2c, 2k and 2l, the transmission coefficients of spin up and down are the same around E_F, and result in zero SP. For the configurations in Figures 2a and 2b, the transmission is partially polarized. Interestingly, the SP is exactly –33.3%, i.e., 1/3, in a large energy range, as shown in Figures 2e and 2f. One could easily find the transmission coefficients of spin up and down are non-zero-integer values (the spin up is 1 and the spin down is 2), which actually accounts for the constant SP. Although they show partially polarized transmission, the constant SP in a large energy range is also beneficial to the spintronics devices.

Apparently, the spin polarization of transmission is sensitive to the type of the edges. To gain insight into the underlying mechanism, we take the two configurations, BB_{sy}@8-$ZFeB_2$NR and FeB_{as}@7-$ZFeB_2$NR, as examples to investigate their electronic structures. The band structure and the density of states (DOS) of them are shown in Figure 3. For BB_{sy}@8-$ZFeB_2$NR in Figure 3a, there is a band across E_F for each spin. As a result, the DOS of it is spin unpolarized around E_F, see the left panel of Figure 3a. These two bands actually contribute to the spin up and down transmission eigenchannels respectively, and result in the transmission coefficient of 1.0 for each spin, see Figure 2c. Consequently, the SP is zero.

To figure out the origin of these states, we calculate the projected density of states (PDOS) for BB_{sy}@8-$ZFeB_2$NR.

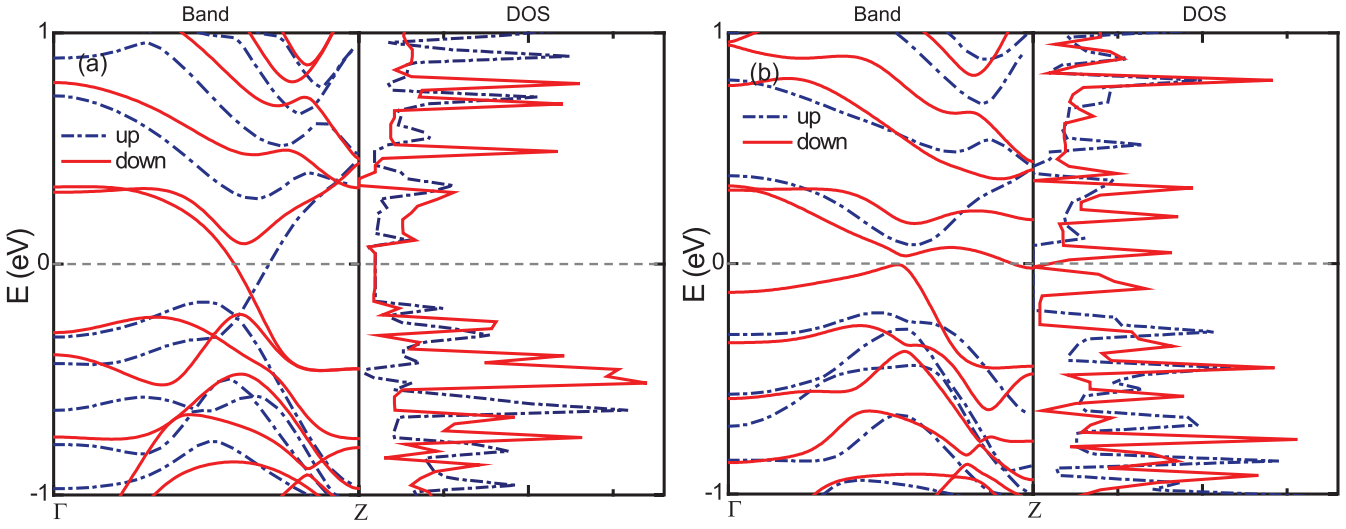

Fig. 3. Electronic structure of $ZFeB_2NRs$. (a, b) Band structure and density of states for BB_{sy}@8-$ZFeB_2NR$ (left panel) and FeB_{as}@7-$ZFeB_2NR$ (right panel), respectively. The blue dashed dot line denotes the spin-up band structure, and the red solid line denotes the spin down band structure. The Fermi level is set to $E_F = 0$.

Figure 4a shows the spin-resolved PDOS projected on all atoms' (including Fe) s and p orbitals. Figures 4b and 4c show the PDOS projected on middle and (near) edge Fe atoms' d orbitals respectively (there are only two (near) edge Fe atoms, and the others are denoted as middle Fe atoms). As there is no d electron in B atoms, the sum of these three PDOS is actually the DOS of the whole system, which is shown in Figure 3a. Obviously, the states around E_F mainly come from the d orbitals of (near) edge Fe atoms, see Figure 4c. A parallel analysis is also performed for FeB_{as}@7-$ZFeB_2NR$, and the same conclusion is drawn, where the states around E_F are contributed by (near) edge Fe atoms' d orbitals, see Figures 4d–4f.

As two examples, BB_{sy}@8-$ZFeB_2NR$ and FeB_{as}@7-$ZFeB_2NR$ show us small change in structure could result in large difference in spin polarization of the transmission. From structural point of view, BB_{sy}@8-$ZFeB_2NR$ only have one more B atom on the edge than FeB_{as}@7-$ZFeB_2NR$ in a unit cell. However, the transmission of the former one is completely spin-unpolarized, and that of the latter one is completely spin-polarized at E_F, see Figures 2g and 2m. In other words, the SP changes from 0 to –100%. Such a modulation is quite beneficial to the design of the spintronic devices. As discussed above, the states around E_F and corresponding transmission channels are mainly contributed by (near) edge Fe atoms, not by B atoms. In these two configurations, the number of Fe atoms are the same, but, surprisingly, the transmission and SP change quite a lot. So it is interesting to figure out the mechanism behind.

Kou et al. have reported that in borophane the hinge dihedral angles' variation, which may arises from strain, would result in the switch of the transport channels [34]. Similar to borophane, monolayer FeB_2 also possesses puckered triangle hinge structure [35,36]. When cutting into nanoribbons, there will be reconstruction around the edges, which would induce changes of hinge dihedral angles. Easy to know, different edges may result in different hinge dihedral angles. To confirm that, we plot the side views of BB_{sy}@8-$ZFeB_2NR$ and FeB_{as}@7-$ZFeB_2NR$, and calculate hinge dihedral angles for all the configurations studies above, shown in Figures 5c and 5d and Table 1 respectively. For clarity, the hinge dihedral angle in this work refers to the dihedral angle of θ shown in Figure 5f.

Due to the release of stain, all the ribbons become curved, not flat like infinite ones. From Figure 5d, one easily finds BB_{sy}@8-$ZFeB_2NR$ has a mirror symmetry. Its hinge dihedral angles are almost the same, distributed in the small range of [148.55°, 148.66°]. The transmissions are the same for spin up and down. After removing the outermost B atoms on the left edge, we get FeB_{as}@7-$ZFeB_2NR$. Comparing with BB_{sy}@8-$ZFeB_2NR$, the right three hinge dihedral angles are slightly affected and they become 152.21°, 149.55° and 149.32° respectively. However, the left hinge dihedral angle changes quite a lot, and it becomes 115.76°, see Figure 5c. There is no mirror symmetry in the transverse direction any more. According to the channel's switching effect, [34] the variation would influence and even switch off the transmission channels. As a result, the spin up channel is totally blocked. But such a effect is not sensitive to the spin down channel, which is not turned off. So the SP becomes –100%. In the following, we will show that it is actually the symmetry of the distribution of the hinge dihedral angles that results in the different switching effect for opposite spins, not the symmetry of the ribbon itself.

Next, we choose four configurations in each terminated-edge category (BB-, FeB- and FeFe-terminated ones), and calculate their dihedral angles and SP, shown in Table 1. For the FeB-terminated ribbons, the left dihedral angles are distributed in [115.42°, 116.03°], much smaller than the right dihedral angles, which are in the range of [148.57°, 157.38°]. The switching effect in them works well and the SPs are all –100%, although the ribbon's width

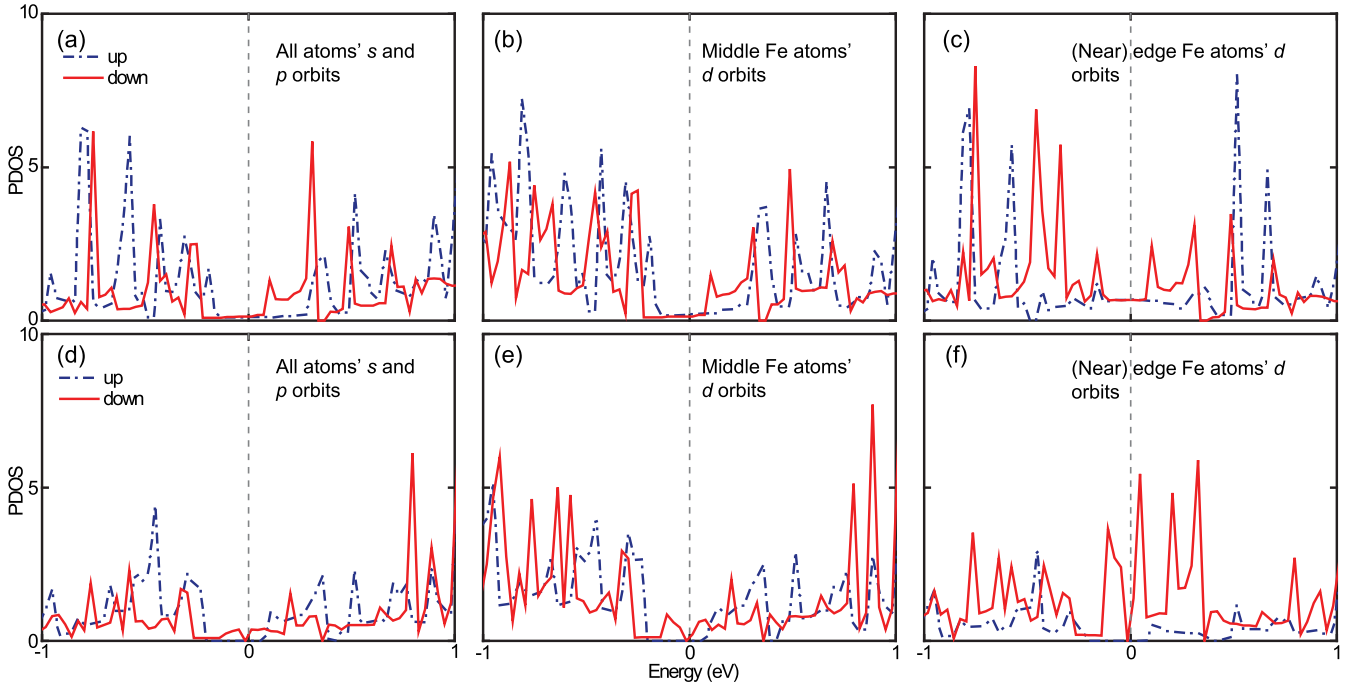

Fig. 4. (a–c) PDOS of BB_{sy}@8-$ZFeB_2$NR projected on (a) all atoms' s and p orbitals, (b) middle Fe atoms' d orbitals and (c) (near) edge Fe atoms' d orbitals, respectively. (d–f) PDOS of FeB_{as}@7-$ZFeB_2$NR projected on (a) all atoms' s and p orbitals, (b) middle Fe atoms' d orbitals and (c) (near) edge Fe atoms' d orbitals, respectively.

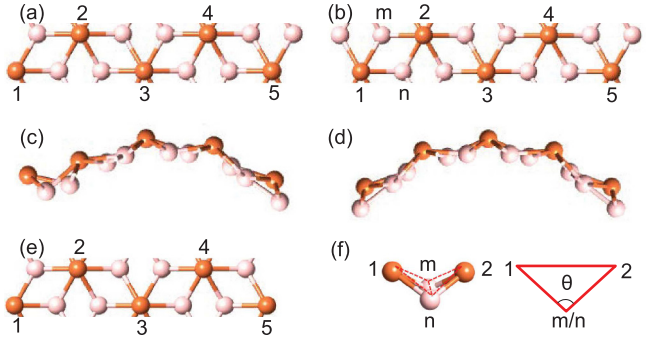

Fig. 5. The structures of FeB_{as}@7-$ZFeB_2$NRs. (a) Top view of FeB_{as}@7-$ZFeB_2$NR. (b) Top view of BB_{sy}@8-$ZFeB_2$NR. (c) and (d) Side views of the configurations in (a) and (b) respectively. (e) Top view of $FeFe_{sy}$@7-$ZFeB_2$NR. To see clearly, the structures of (a), (b) and (e) are used the flat structure cutting from the infinite ribbon (before optimization), and the optimized structures are curved. (f) The hinge dihedral angle of θ studied in this work in $ZFeB_2$NRs, where atoms m and n are on the intersection line of the two faces.

varies. That is to say, such an effect is robust to the width of the ribbon, showing great application potential.

Interestingly, for FeFe-terminated configurations, no matter what the ribbon's symmetry and width are, the SP is zero, see Class III in Table 1. There is no correspondence between ribbon's symmetry and spin-polarized state of the transmission. This is quite different from the above two categories, where symmetric/asymmetric configuration induces spin-unpolarized/polarized transmission. As discussed before, the transmission channels are mainly contributed by the states around (near) edge Fe atoms, and the channel is switched by the Fe-involved dihedral angles. So we should pay attention to the symmetry of these dihedral angles, not the symmetry of the ribbon. In Table 1, we give out the symmetry of the distribution of the hinge dihedral angles in the transverse direction of the ribbon. Surprisingly, there exists a one-to-one correspondence between the symmetry of the angles' distribution and the spin-polarized state of the transmission, where symmetric/asymmetric distribution triggers spin-unpolarized/polarized transmission. And this correspondence is not only valid for FeFe-terminated cases, but also valid for all the configurations. Moreover, it is robust to ribbon's symmetry and width. For examples, both $FeFe_{as}$@5-$ZFeB_2$NR and $FeFe_{sy}$@7-$ZFeB_2$NR can induce spin-unpolarized transmission, although one of them is asymmetric and the other one is symmetric, see the insets in Figures 2k and 2l. Because the dihedral angles' distributions of them are both symmetric. Apparently, the symmetry of the distribution of the dihedral angles is the key point, which modulates the spin-polarization of the transmission. We believe our findings are quite useful for the development of B-based spintronic devices.

It should be noted that, for asymmetric BB-terminated configurations (such as BB_{as}@7-$ZFeB_2$NR), the difference between the left and right dihedral angles are much smaller than that of FeB-terminated cases. Although the distribution of the dihedral angles is asymmetric, which should induce spin-polarized transmission, the smaller difference only results in SP = –33.3%. In other words, the asymmetry is not large enough to trigger a SP of –100%

Table 1. Hinge dihedral angles (from left to right along the transverse direction of the ribbon), the symmetry of the distribution of these angles (note the symmetry here does not refer to the symmetry of the ribbon's geometry), and the spin polarization of transmission for each configuration, respectively.

	Configuration	Dihedral angles						Symmetry	SP (%)
	BB_{as}@5-$ZFeB_2NR$	147.58°	156.53°					Asymmetric	–33.33
Class I	BB_{as}@7-$ZFeB_2NR$	149.65°	149.64°	158.15°				Asymmetric	–33.33
	BB_{as}@8-$ZFeB_2NR$	149.35°	149.88°	147.77°	157.16°			Asymmetric	–33.33
	BB_{sy}@8-$ZFeB_2NR$	148.66°	148.55°	148.58°	148.58°			Symmetric	0
	FeB_{as}@6-$ZFeB_2NR$	115.42°	151.49°	156.22°				Asymmetric	–100
Class II	FeB_{as}@7-$ZFeB_2NR$	115.76°	152.21°	149.55°	149.32°			Asymmetric	–100
	FeB_{as}@8-$ZFeB_2NR$	115.71°	152.93°	147.50°	157.38°			Asymmetric	–100
	FeB_{as}@9-$ZFeB_2NR$	116.03°	151.99°	147.62°	148.91°	148.57°		Asymmetric	–100
	$FeFe_{as}$@5-$ZFeB_2NR$	115.62°	153.99°	115.63°				Symmetric	0
Class III	$FeFe_{sy}$@7-$ZFeB_2NR$	115.58°	150.91°	150.83°	115.63°			Symmetric	0
	$FeFe_{as}$@8-$ZFeB_2NR$	115.75°	151.72°	145.63°	151.38°	115.77°		Symmetric	0
	$FeFe_{sy}$@10-$ZFeB_2NR$	115.51°	147.77°	133.81°	133.79°	147.75°	115.48°	Symmetric	0

like FeB-terminated cases. Due to the presence of Fe-3*d* orbitals, we examined the band structure and density of states for BB_{sy}@8-$ZFeB_2NR$ and FeB_{as}@7-$ZFeB_2NR$ by employing GGA+U (the figures are not shown). We choose U to be 4.0 eV to check the effect of it on the electronic properties of $ZFeB_2NR$ [37–39]. For the configuration of BB_{sy}@8-$ZFeB_2NR$ under GGA+U, it is found that there are both spin-up and spin-down bands across E_F, which exhibits metallity. And the DOS of it is spin unpolarized around E_F. These are consistent with the results without U in the above. For the configuration of FeB_{as}@7-$ZFeB_2NR$ under GGA+U, there exist a spin-down band across E_F and a band gap in the spin-up component, which exhibit half-metallity and 100% spin polarization around the Fermi level. They are also consistent with the results without U, see Figure 3b. In short, the U effect has little influence on the conclusions of our work. Moreover, we also investigate the effect the hydrogen passivation of the edge in $ZFeB_2NR$. It is found that the hydrogen passivation on the edge has little effect on the electronic properties.

4 Conclusion

To summarize, we investigate the spin-dependent transport properties of $ZFeB_2NR$s using first-principles calculations. It is found that, around E_F, FeB-terminated $ZFeB_2NR$s exhibit completely spin-polarized transmission, but FeFe-terminated ones exhibit completely spin unpolarized transmission. In addition, BB-terminated cases exhibit partially spin-polarized or completely spin-unpolarized transmission, depending on the geometry of the ribbon. Further analysis shows that, the hinge dihedral angle has a switching effect on the transport channels, but its influence on opposite spins is sensitive to the symmetry of the angles' distribution along the transverse direction (not the symmetry of the ribbon), where symmetric/asymmetric distribution induces spin-unpolarized/polarized transmission. Moreover, calculation shows that such a symmetry effect is robust to the edge type and the width of the ribbon, showing great application potential. As the spin polarization could vary from completely unpolarized (0) to completely polarized (–100%), our results are quite useful for the manipulation of a spin current in future boron-based spintronic devices.

This work is supported by the National Natural Science Foundation of China (NSFC11504178), the Natural Science Foundation of Jiangsu Province (BK20150825), the Scientific Research Foundation of Nanjing University of Posts and Telecommunications (NY217013), and Natural Science Found for Colleges and Universities in Jiangsu Province (17KJB140015).

Author contribution statement

Jian-Hua Li performs the calculations and writes the paper. Yan-Dong Guo and Xiao-Hong Yan supervise the project. Others contribute to discussions on the mechanism of the spin polarization and also revise the paper.

References

1. D.D. Awschalom, M.E. Flatté, Nat. Phys. **3**, 153 (2007)
2. S.A. Wolf, D.D. Awschalom, R.A. Buhrman, J.M. Daughton, S. Von Molnar, M.L. Roukes, A. Chtchelkanova, D.M. Treger, Science **294**, 1488 (2001)
3. D.C. Worledge, Appl. Phys. Lett. **84**, 4559 (2004)
4. S. Stankovich, D.A. Dikin, R.D. Piner, K.A. Kohlhaas, A. Kleinhammes, Y. Jia, Y. Wu, S.T. Nguyen, R.S. Ruoff, Carbon **45**, 1558 (2007)
5. Y.D. Guo, X.H. Yan, Y. Xiao, J. Appl. Phys. **113**, 244302 (2013)
6. Y.D. Guo, X.H. Yan, Y. Xiao, J. Appl. Phys. **108**, 104309 (2010)
7. H.C. Schniepp, J.-L. Li, M.J. McAllister, H. Sai, H.-A. Hiroaki, A. Margarita, H. Douglas, R.K. Prud'homme, R. Car, D.A. Saville, I.A. Aksay, J. Phys. Chem. B **110**, 8535 (2006)
8. M.Y Han, B. Özyilmaz, Y. Zhang, P. Kim, Phys. Rev. Lett. **98**, 206805 (2007)
9. A.J. Mannix et al., Science **350**, 1513 (2015)

10. Z. Zhang, Y. Yang, G. Gao, B.I. Yakobson, Angew. Chem. Int. Ed. **54**, 13022 (2015)
11. H. Zhang, Y. Li, J. Hou, A. Du, Z. Chen, Nano Lett. **16**, 6124 (2016)
12. K. Nakada, M. Fujita, G. Dresselhaus, M.S. Dresselhaus, Phys. Rev. B **54**, 17954 (1996)
13. Y. Kobayashi, K.I. Fukui, T. Enoki, K. Kusakabe, Phys. Rev. B **73**, 125415 (2006)
14. H. Pan, Y.-W. Zhang, J. Mater. Chem. **22**, 7280 (2012)
15. Y.-W. Son, M.L. Cohen, S.G. Louie, Phys. Rev. Lett. **97**, 216803 (2006)
16. Y. An, M. Zhang, L. Chen, C. Xia, T. Wang, Z. Fu, Z. Jiao, G. Xu, RSC Adv. **5**, 107136 (2015)
17. E.-J. Kan, Z. Li, J. Yang, J.G. Hou, J. Am. Chem. Soc. **130**, 4224 (2008)
18. S. Majumdar, R. Laiho, P. Laukkanen, I.J. Väyrynen, H.S. Majumdar, R. Österbacka, Appl. Phys. Lett. **89**, 122114 (2006)
19. J. Taylor, H. Guo, J. Wang, Phys. Rev. B **63**, 245407 (2001)
20. M. Brandbyge, J. Mozos, P. Ordejón, J. Taylor, K. Stokbro, Phys. Rev. B **65**, 165401 (2002)
21. F.D. Novaes, A.J.R. Silva, A. Fazzio, Braz. J. Phys. **36**, 799 (2006)
22. S. Datta, Superlattice Microstruct. **28**, 253 (2000)
23. A.J. Cohen, P. Mori-Sánchez, W. Yang, Science **321**, 792 (2008)
24. http://www.quantumwise.com/
25. J.P. Perdew, K. Burke and M. Ernzerhof, Phys. Rev. Lett. **77**, 3865 (1996)
26. J.P. Perdew, J.A. Chevary, S.H. Vosko, K.A. Jackson, M.R. Pederson, D.J. Singh, C. Fiolhais, Phys. Rev. B **46**, 6671 (1992)
27. T.B. Martins, R.H. Miwa, A.J.R. Da Silva, A. Fazzio, Phys. Rev. Lett. **98**, 196803 (2007)
28. F. Cervantes-Sodi, G. Csanyi, S. Piscanec, A.C. Ferrari, Phys. Rev. B **77**, 165427 (2008)
29. K. Sato, H. Katayama-Yoshida, Jpn J. Appl. Phys. **40**, L334 (2001)
30. S. Okada, A. Oshiyama, Phys. Rev. Lett. **87**, 146803 (2001)
31. S. Datta, *Electronic transport in mesoscopic systems* (Cambridge University Press, 1997)
32. L. Levitov, D.A. Case, Adv. Inorg. Chem. **38**, 423 (1992)
33. D.A. Abanin, P.A. Lee, L.S. Levitov, Phys. Rev. Lett. **96**, 176803 (2006)
34. L. Kou, Y. Ma, C. Tang, Z. Sun, A. Du, C. Chen, Nano Lett. **16**, 7910 (2016)
35. J. Zhang, H.J. Liu, L. Cheng, J. Wei, J.H. Liang, D.D. Fan, J. Shi, X.F. Tang, Q.J. Zhang, Sci. Rep. **4**, 6452 (2014)
36. J. Padilha, R.H. Miwa, A. Fazzio, Phys. Chem. Chem. Phys. **18**, 25491 (2016)
37. M. Bernien et al., Phys. Rev. B **102**, 047202 (2009)
38. L. Wang, T. Maxisch, G. Ceder, Phys. Rev. B **73**, 195107 (2006)
39. J. Zhou, Q. Sun, J. Am. Chem. Soc. **133**, 15113 (2011)